Carbohydrate Polymers 267 (2021) 118156

Contents lists available at ScienceDirect

Carbohydrate Polymers

journal homepage: www.elsevier.com/locate/carbpol

Chitosan scaffolds with enhanced mechanical strength and elastic response by combination of freeze gelation, photo-crosslinking and freeze-drying

Ilaria Silvestro [a], Riccardo Sergi [a], Anna Scotto D'Abusco [b], Alessia Mariano [b], Andrea Martinelli [a], Antonella Piozzi [a], Iolanda Francolini [a,*]

[a] Department of Chemistry, Sapienza University of Rome, Italy
[b] Department of Biochemical Sciences, Sapienza University of Rome, Italy.

ARTICLE INFO

Keywords:
Scaffolds
Tissue engineering
Chitosan
Fabrication method
Mechanical properties

ABSTRACT

In this study, a new scaffold fabrication method based on the combination of a series of stabilization processes was set up to obtain chitosan scaffolds with improved mechanical properties for regeneration of load-bearing tissues. Specifically, thermally induced phase separation (TIPS) of chitosan solutions was used to obtain an open structure which was then stabilized by freeze-gelation and photo cross-linking. Freeze-gelation combined with freeze-drying permitted to obtain a porous structure with a 95 μm-mean pore size suitable for osteoblast cells' housing. Photo-crosslinking improved by ca. three times the scaffold compressive modulus, passing from 0,8 MPa of the uncrosslinked scaffolds to 2,2 MPa of the crosslinked one. Hydrated crosslinked scaffolds showed a good elastic response, with an 80% elastic recovery for at least 5 consecutive compressive cycles. The herein reported method has the advantage to not require the use of potentially toxic cross-linking agents and may be extended to other soft materials.

1. Introduction

Tissue engineering is a very promising approach to in vivo regenerate damaged tissues. Such approach relies on the seeding of cells into biocompatible and biodegradable porous scaffolds, acting as temporary biological and mechanical supports for cell adhesion and tissue growth. The structure of the scaffolds plays a pivotal role for the success of tissue regeneration since it should provide an environment able to mimicking the extracellular matrix in terms of porosity, pore interconnection and mechanical stability. Specifically, under a functional point of view, the scaffold should keep a structural integrity for all tissue regeneration course and ensure a mechanical response coherent with the replaced tissue. A proper mechanical response is crucial for regeneration of load-bearing tissues, like bones or cartilages, but also for replacement of non-load bearing soft tissues submitted to repeated and cyclical stresses like heart valves. Besides that, recently, a correlation between scaffold stiffness and cell behavior has been also demonstrated (Dado & Levenberg, 2009).

Polysaccharides are considered among the best materials for tissue regeneration because of their excellent biodegradability, biocompatibility, and bioactivity. However, these soft materials often suffer from poor mechanical resistance and low stability in water environment, which may compromise their in-use performance. That's also the case of chitosan, a natural polycation deriving from the partial deacetylation of chitin, largely investigated for biomedical applications, because of its outstanding biological properties including mucoadhesivity and antimicrobial properties (Amato et al., 2018; Cuzzucoli Crucitti et al., 2018; Francolini, Donelli, Crisante, Taresco, & Piozzi, 2015; Silvestro et al., 2020; Wang et al., 2020). Additionally, more than other natural polymers, chitosan triggers a minimal foreign-body response and fibrous encapsulation (Bhattarai, Edmondson, Veiseh, Matsen, & Zhang, 2005; Jayakumar, Prabaharan, Nair, & Tamura, 2010; Kim et al., 2008). Chitosan has been shown to be especially attractive as a scaffold material for bone regeneration due to its in vitro ability to support adhesion and proliferation of osteoblasts as well as promote formation of mineralized bone matrix (Aguilar et al., 2019; Seol et al., 2004). Indeed, chitosan, together with hydroxyapatite, is among the very few osteoconductive materials considered promising for bone tissue engineering (Venkatesan

* Corresponding author at: Sapienza University of Rome, Department of Chemistry, Piazzale Aldo Moro, 5, 00185 Rome, Italy.
E-mail addresses: ilaria.silvestro@uniroma1.it (I. Silvestro), sergi.1714031@studenti.uniroma1.it (R. Sergi), anna.scottodabusco@uniroma1.it (A.S. D'Abusco), alessia.mariano@uniroma1.it (A. Mariano), andrea.martinelli@uniroma1.it (A. Martinelli), antonella.piozzi@uniroma1.it (A. Piozzi), iolanda.francolini@uniroma1.it (I. Francolini).

https://doi.org/10.1016/j.carbpol.2021.118156
Received 30 December 2020; Received in revised form 1 April 2021; Accepted 16 April 2021
Available online 7 May 2021

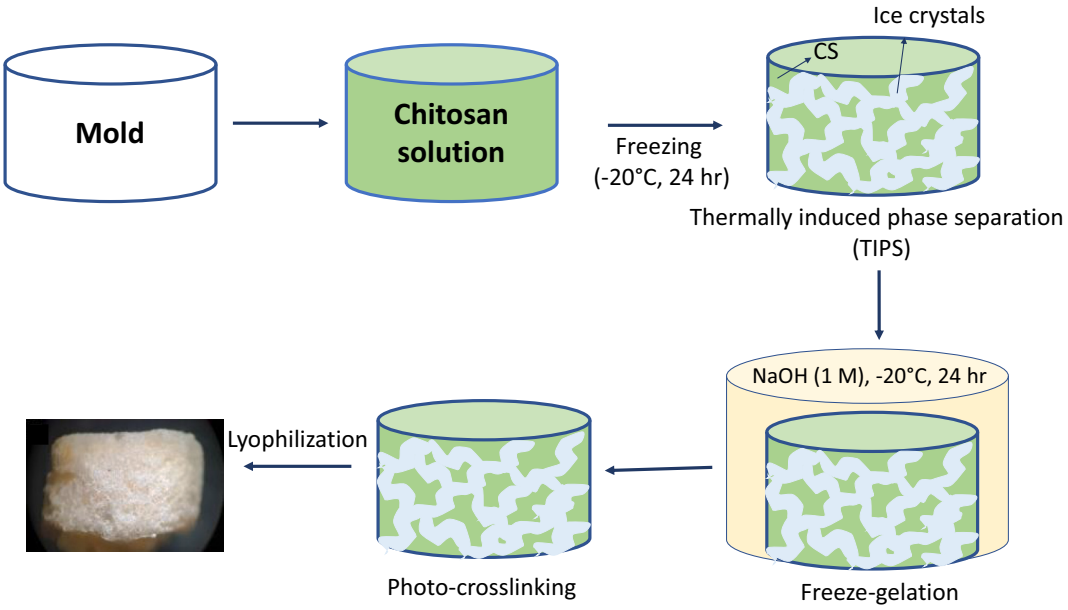

Fig. 1. Scheme of the whole process used to obtain reinforced chitosan scaffolds.

& Kim, 2010). Chitosan scaffolds have been also proposed for cardiac tissue engineering and regeneration by proper modulation of their mechanical properties (Esmaeili Pourfarhangi, Mashayekhan, Asl, & Hajebrahimi, 2018).

A number of studies has been lately focused on improvement of mechanical properties of chitosan-based scaffolds mainly through chemical cross-linking (Ma et al., 2003; Wu et al., 2018), blending with polymers (Pineda-Castillo et al., 2018) or proteins (Chollakup, Uttayarat, Chworos, & Smitthipong, 2020), complexing with DNA (Pakornpadungsit, Prasopdee, Swainson, Chworos, & Smitthipong, 2020) and addition of reinforcement fillers (Arumugam et al., 2020; Francolini et al., 2019; Jabbari, Hesaraki, & Houshmand, 2019). However, while the use of chemical cross-linkers may cause undesired toxic effects on cells, the use of reinforcing fillers may alter the biological properties of chitosan especially when used at high contents (Albanna, Bou-Akl, Blowytsky, & Matthew, 2012). Other approaches include formation of physical ionic networks through interaction with anionic molecules (Xu et al., 2018), even if in some cases improvements in the scaffold mechanical properties have been found to be low.

In this framework, herein we report the setup of a new fabrication method to obtain chitosan scaffolds with improved mechanical properties based on the combination of a series of stabilization processes. Specifically, a thermally induced phase separation (TIPS) of chitosan solutions at different concentrations was applied to produce a porous structure. One of the advantages of TIPS is that the scaffold porous structures may be easily tuned by varying several thermodynamic and kinetics parameters. However, differently from the common procedure described in the literature, which involves just sample freeze-drying, in our study, two stages of stabilization were added after TIPS, before freeze drying, which are gelation in NaOH under freezing condition (freeze-gelation) and photo cross-linking. Our hypothesis was that polymer gelling and neutralization in freezing conditions could limit a potential structure collapse induced by the heat released during the neutralization reaction. Besides, we also hypothesized that photo cross-linking could contribute to the structure stabilization without the use of chemical cross-linkers. The mechanical properties of the scaffolds were investigated by cyclic compression tests performed on both dried and hydrated samples. The morphology of the scaffolds was observed by field emission scanning electron microscopy while porosity and pore interconnection were evaluated by the liquid displacement method. Finally, osteoblast cells were seeded onto the chitosan scaffolds to confirm suitability of the obtained structures for cell housing.

2. Materials and methods

2.1. Materials

Chitosan (CS, medium molecular weight, 200–800 cP at 1 wt% in 1% acetic acid at 25 °C, 75%–85% deacetylated), acetic acid, sodium hydroxide (NaOH), and IRGACURE D-2959 (2-hydroxy-4′-(2-hydroxyethoxy)-2-methylpropiophenone) were purchased from Sigma Aldrich (Darmstadt, Germany). All chemicals were of analytical grade and were used without further purification.

2.2. Preparation of chitosan scaffolds

Chitosan was dissolved in 2% acetic acid (0.35 M) at variable concentrations by magnetic stirring and sonication. Before use, CS solutions were centrifugated and dialyzed in water (membrane cutoff 3.5 kDa) for 24 h. Then, 2 mL aliquots of CS solutions were put into cylindric polystyrene molds (d = 2,5 cm, h = 1 cm) and frozen at −20 °C per 24 h, as previously described (Nam & Park, 1999). In this phase, a thermally induced phase separation (TIPS) occurs causing demixing of the homogeneous CS/solvent solution into a polymer-rich acetic acid phase and water-ice phase that once freeze-dried produces a porous structure. Then, the frozen cylinders were put in contact with 2 mL of a NaOH solution in ethanol (1 M or 3 M) for 24 h at −20 °C in order to achieve polymer gelling and extraction of acetic acid solution (Hsieh et al., 2007). Then, the scaffold open structure was submitted to different treatments: ***Procedure A)*** slow drying at room temperature. Scaffolds were named CSX_NaY where X is the chitosan solution concentration (2, 4 or 6%) and Y is NaOH concentration (1 or 3 M) used for freeze-gelation. ***Procedure B)*** freeze-drying. Scaffolds were named CSX_FD where X is the chitosan solution concentration while FD stands for freeze-drying. ***Procedure C)*** UV crosslinking (λ =254 nm, 10 min) and freeze-drying. IRGACURE D-2959 (2% wt/wt) was used as photo-initiator. Scaffolds were named as CSX_FD_CL where X is the chitosan solution concentration while FD and CL stand for freeze-drying and cross-linking, respectively. In Fig. 1, a scheme of the entire process is reported.

2.3. Evaluation of chitosan photo cross-linking

Photo cross-linked chitosan scaffolds were characterized by Infrared Spectroscopy (IR), thermogravimetric analysis (TGA) and soluble fraction in order to evaluate possible variations of scaffold properties induced by photo irradiation with respect to the freeze-dried uncrossliked scaffolds. IR spectra were acquired in Attenuated Total Reflection (ATR) by a Nicolet 6700 (Thermo Fisher Scientific, USA) equipped with a Golden Gate ATR accessory, at a resolution of 2 cm^{-1} and co-adding 100 scans. TGA was carried out by using a Mettler TG50 thermobalance (Mettler Toledo, USA), in the 25÷500 °C temperature range, at a 10 °C min^{-1} heating rate and under N_2 flow. The scaffold soluble fraction was evaluated in PBS butter at 37 °C. Specifically, weighted scaffolds (W_0) were immersed in PBS for 24 h, 48 h and 72 h. At each time, the scaffold was withdrawn, dried in vacuum oven at 37 °C and weighted (W_t). The soluble fraction (SF) was determined as follow:

$$SF = \frac{W_0 - W_t}{W_0}$$

2.4. Determination of scaffolds' porosity

Scaffolds total porosity was determined by the liquid displacement method as reported by Zeng et al. (2015). Ethanol was used as the displacement liquid because, being a chitosan non-solvent, it can penetrate into the porous structure without inducing scaffold morphological variation like shrinkage or swelling. Scaffolds (dry mass M_0) were immersed for 1 h in a known volume of ethanol. The weight of the whole system (scaffold + ethanol) was recorded (M_a). Then, the scaffold was removed, and the remaining ethanol was weighted (M_b). Meanwhile, a calibrated container was filled with ethanol and weighed (M_1). Then, the calibrated container was emptied and the wet scaffold previously soaked in ethanol was placed in the container. Ethanol was then added until the container was filled to the same mark. The container was finally weighed again (M_2).

Porosity was calculated according to the following equations where ρ is the density of ethanol (0.806 g/cm^3 at 20 °C):

Volume of scaffold pores: $V_1 = \frac{M_a - M_b - M_0}{\rho}$

Apparent volume of the scaffold: $V_2 = \frac{(M_a - M_b) - (M_2 - M_1)}{\rho}$

Porosity of the scaffold (P, %): $P = \frac{V_1}{V_2} x\,100 = \frac{(M_a - M_b - M_0)}{(M_a - M_b) - (M_2 - M_1)} x\,100$

2.5. Evaluation of scaffold morphology

The scaffold morphology and microstructure were observed by field emission scanning electron microscope (FESEM, AURIGA Zeiss). Both scaffold surface and bulk morphology were observed. For observation of the scaffold bulk structure, scaffolds were fractured in liquid nitrogen. For analysis, samples were fixed onto stubs and gold sputtered. Images were analyzed with the ImageJ software to determine the scaffold mean pore size and pore size distribution.

2.6. Scaffold swelling ability

The kinetics of scaffold water uptake was determined at room temperature in water. At determined times, scaffolds were removed from water and weighed, after removal of the water excess by blotting with a filter paper. The analysis was repeated until a constant weight (equilibrium swelling weight, W^*) was reached. The swelling ratio (SR) was determined as following:

$$SR = \left(\frac{W_t - W_0}{W_0}\right)$$

where W_t is the sample weight after swelling at time t and W_0 is the sample initial weight. Three parallel swelling experiments were performed for each sample and data were reported as average value ± standard deviation (SD).

2.7. Mechanical tests in compression

The mechanical behavior of the scaffolds was investigated by performing compressive tests on both dried and hydrated samples. Specifically, cylindrical scaffolds (2 cm average diameter and 1 cm average height) have been placed between the two flat plates of the ISTRON 4502 instrument. Then, a crosshead speed of the top INSTRON plate was set at 1 mm/min and the load was applied until 50% reduction in specimen height. The compressive modulus (CM) was determined from the slope of the initial linear tract of the curve (until 10% of deformation) while the maximum compressive strength was determined before the Yield Point, in correspondence of a 30% compression ratio, that is the irreversible deformation of the structure. Five parallel samples were tested for every scaffold, and mechanical properties were reported as average value ± SD.

To estimate the scaffold fatigue life, five consecutive cycles of compression were performed on each scaffold, setting 0.5 as the maximum compression ratio in each cycle. Tenacity (T) of the scaffold at each compression cycle was evaluated by determining the area of the stress-strain curve while the elastic recovery (ER, %) after each compression cycle was determined by the following equation:

$$ER\ (\%) = \frac{T_x}{T_1} \text{ x } 100$$

where x is the cycle number and T_1 is the tenacity at the cycle 1.

2.8. Cell viability tests

To investigate the suitability of the obtained porous chitosan scaffold to house cells, human primary osteoblast (hOB) cells were used. hOB cells were isolated as previously described (Lopreiato et al., 2020). Scaffolds were set down into 96 well tissue culture plate and conditioned in DMEM without red phenol supplemented with L-glutamine, penicillin/streptomycin, Na-pyruvate, non-essential aminoacids, plus 10% Fetal Bovine Serum (FBS) for 2 h at 37 °C, in 95% humidity and 5% CO_2 atmosphere. Then, cells (2×10^4) were added into the wells containing the scaffolds and forced to penetrate into the porous scaffolds by compressing the scaffold inside the cell suspension (sponge effect). Cells were also seeded into a plate well without scaffold as negative control while cells treated with 1.0% (v/v) Triton X-100 served as positive control. Following incubation at 37 °C in 95% humidity and 5% CO_2 atmosphere for 48 h, viability of cells grown onto the polystyrene plate or penetrated into the scaffold was evaluated by measuring the mitochondrial dehydrogenase activity using the dye 3-(4,5-dimethylthiazol-2-yl)-5-(3-carboxymethoxyphenyl)2-(4-sulfophenyl)-2H-tetrazolium (MTS) (Promega Corporation, Madison, WI, USA). Briefly, the MTS dye was put in contact either with cells grown onto the polystyrene plate or with the scaffold containing the cells and cultured for 4 h to allow the formation of formazan crystals by viable cells. The colour variation of the scaffold was monitored as an indication of cell viability, by measuring the spectrophotometric absorbance at 492 nm. A CS scaffold not containing cells was also stained with the MTS dye as negative control. The optical density produced by osteoblasts seeded directly into 96 well tissue culture plate was evaluated as 100%. All the experiments were performed in triplicate.

2.9. Evaluation of morphology of cells seeded into scaffold

The morphology of cells seeded into scaffold was observed by field emission scanning electron microscope (FESEM, AURIGA Zeiss). 2×10^4 osteoblasts were seeded into scaffolds as above described and incubated for 48 h. At the end of this incubation, the scaffolds containing the cells were fixed in 2.5% glutaraldehyde in phosphate buffer saline for 3 h,

Table 1
Summary of the procedures adopted for scaffold preparation. Scaffolds' swelling degree (SD), compression modulus (CM) of dried scaffolds, mean pore size and morphology according to FESEM micrographs reported in Figs. 4 and 6. *ND = not determined.

Procedure	Acronym	CS conc. (%)	NaOH conc. (M)	SD (%)	CM (MPa)	Mean pore size (μm)	Morphology
A	CS2_Na3	2	3	315 ± 15	ND*	5 ± 2	Low porosity; Small pores
Drying at 25 °C	CS4_Na3	4	3	270 ± 20	ND	35 ± 13	Low porosity; Small pores
	CS6_Na3	6	3	265 ± 30	ND	–	Compact structure
	CS4_Na1	4	1	330 ± 20	ND	72 ± 33	Larger pores; heterogeneous structure
B	CS4_FD	4	1	920 ± 50	0,80 ± 0.05	105 ± 30	Low pore interconnection
Freeze-drying							
C	CS4_FD_CL	4	1	790 ± 40	2,20 ± 0.10	138 ± 62	Homogeneous and interconnected structure
Freeze-drying / UV cross-linking							

dehydrated through a graded series of ethyl alcohol and treated with hexamethyldisilazane for 10 min. For FESEM analysis, samples were fixed onto stubs and gold sputtered.

2.10. Statistics

Analysis of variance comparisons was performed using Mini-Tab. Differences were considered significant for $p < 0.05$. Data are reported as means ± SD.

3. Results and discussion

Chitosan is classified as bioactive, biodegradable and osteoconductive. Therefore, its application for bone regeneration is very promising if it were not for its poor mechanical strength and structural stability in biological environment. Therefore, the use of chitosan scaffolds for regeneration of load-bearing tissues necessarily requires the development of strategies to improve its compressive modulus, tenacity, and fatigue life.

In this work, a fabrication procedure to obtain chitosan scaffold with improved mechanical properties was set up by combining a series of stabilization processes during scaffold formation. Specifically, a porous structure was first obtained by thermally induced phase separation (TIPS), which is a process related to the decrease in the solvent quality with temperature decrease (van de Witte, Dijkstra, van den Berg, & Feijen, 1996). Indeed, the freezing of a polymer solution causes a thermodynamic demixing of the solution into a polymer-rich phase and a solvent-rich phase. The subsequent growth and coalescence of the polymer-poor phase form the pores in scaffolds, once the solvent is removed, for instance by freeze-drying.

We decided to add two stabilization steps after TIPS, before freeze-drying, which are freeze-gelation and photo cross-linking. Specifically, the combination of liquid-liquid demixing with phase transitions, like polymer gelation, crystallization, or freezing of the solvent may contribute to fix the structure formed during liquid-liquid demixing. Such structure fixation may avoid, during solvent removal, remixing of the phase-separated solution which leads to destruction of the porous structure.

Therefore, in this study, polymer gelation under freezing with NaOH aimed at stabilizing the open structure generated by TIPS. Being NaOH a non-solvent for chitosan, during immersion of the demixed chitosan solution, gelation of chitosan occurs because the good solvent in the polymer solution is exchanged with the nonsolvent. In this way, scaffold porosity can be controlled. NaOH gelation also ensures acetic acid removal from the CS scaffold, which can be toxic for cells as well as can promote dissolution of the scaffold in aqueous environments. Polymer gelation was performed in freezing conditions to limit structure collapse during the exothermic neutralization reaction.

Two NaOH concentrations (1 and 3 M) were used in freeze gelation as well as two scaffold drying procedures, slow drying at room T (procedure A) or freeze-drying (procedure B), were investigated in order to study the effects of such experimental conditions on scaffold morphology. Finally, the scaffold with the best morphology was submitted to photo-crosslinking before freeze-drying to further reinforce the structure. In Table 1, a summary of the adopted procedures is reported together with samples' acronyms.

As far as the scaffolds obtained by freeze gelation with NaOH 3 M and dried at room T (CS2_Na3, CS4_Na3 and CS6_Na3), the use of different CS concentrations did not significantly affect the scaffold swelling degree at the equilibrium (Table 1), which ranged from 265 for CS6_Na3 to 315 for CS2_Na3.

In contrast, the increase in CS concentration negatively affected scaffold porosity which decreased from ca. 50% of CS2_Na3 to 32% of CS6_Na3 (Fig. 2, $p < 0.05$). Such findings evidence how the viscosity of CS concentration strongly affects demixing of CS solution into a polymer-rich phase and a polymer-poor phase during TIPS. Indeed, as

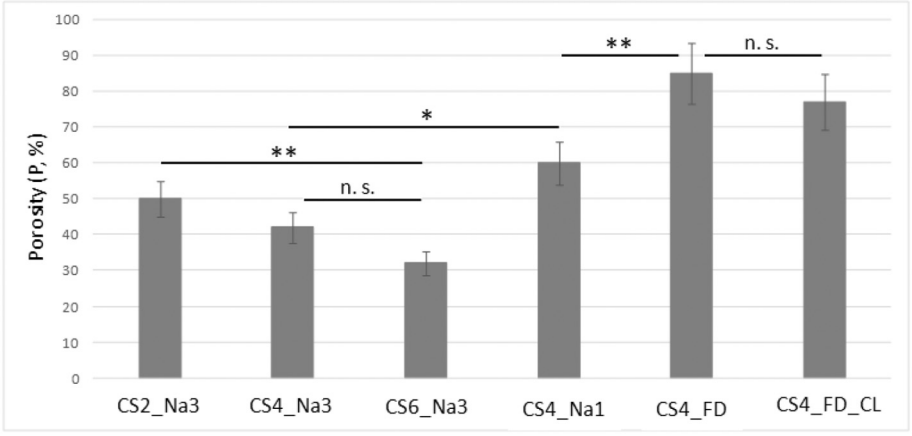

Fig. 2. Porosity (%) of CS scaffolds obtained by the liquid displacement method. CS2_Na3, CS4_Na3, CS6_Na3 obtained by freeze-gelation with NaOH 3 M and dried at room T. CS4_Na1 obtained by freeze-gelation with NaOH 1 M and drying at room T. CS4_FD obtained by freeze-gelation with NaOH 1 M and freeze-drying. CS4_FD_CL obtained by freeze-gelation with NaOH 1 M, photo cross-linking and freeze-drying. Statistical analysis showed a significant difference when *P-value <0.05 and **P-value <0.01. n.s = not significant.

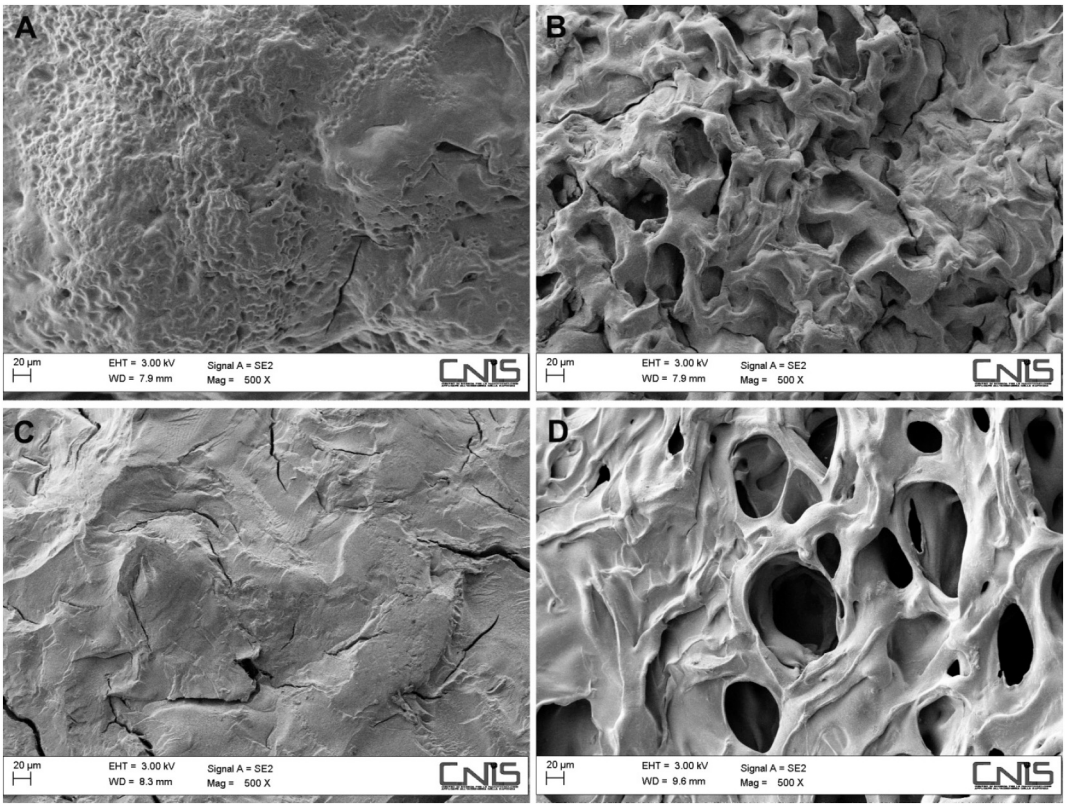

Fig. 3. FESEM micrographs showing the morphology of the CS scaffolds obtained with the procedure A (drying at room T). CS2_NA3 (A), CS4_Na3 (B) and CS6_Na3 (C) obtained by freeze-gelation with NaOH 3 M with a 2%, 4% and 6% CS concentration; CS4_Na1 (D) obtained by freeze-gelation with NaOH 1 M with a 4% CS concentration.

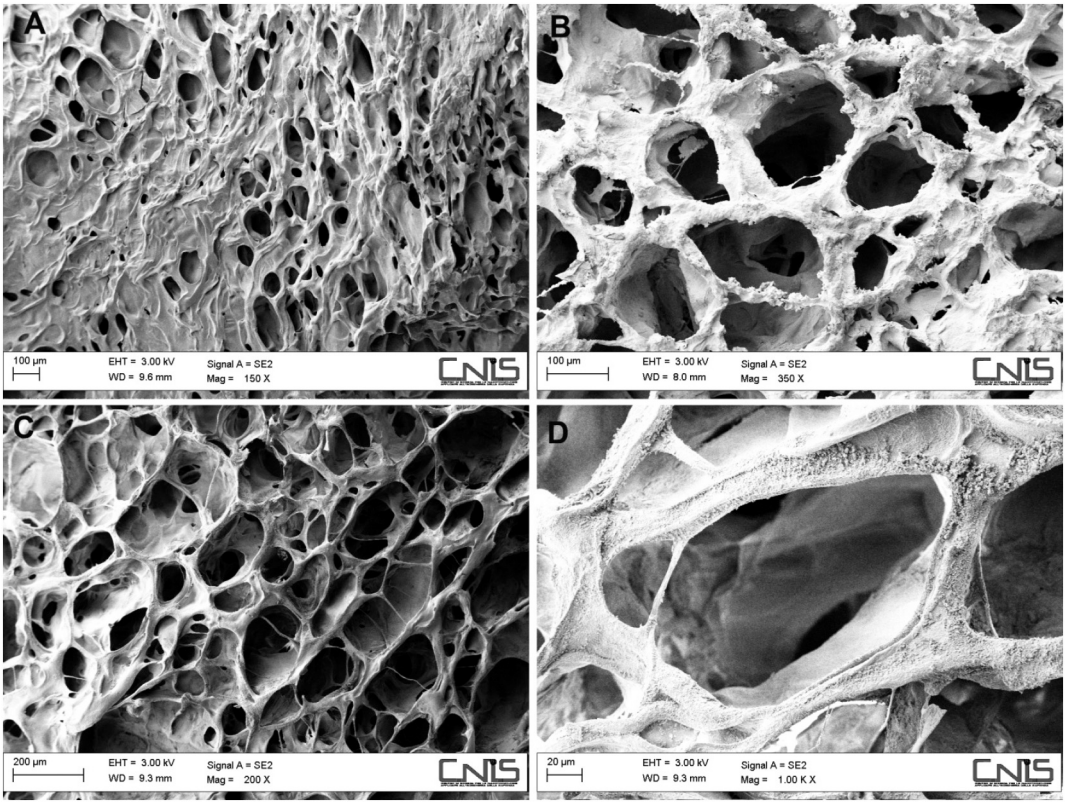

Fig. 4. FESEM micrographs of scaffolds obtained with 4% CS concentration, freeze-gelation with NaOH 1 M and different drying procedures: CS4_Na1 dried at room T (A), CS4_FD freeze-dried (B) and CS4_FD_CL freeze-dried and UV cross-linked observed at 200× magnification (C) and 1000× magnification (D).

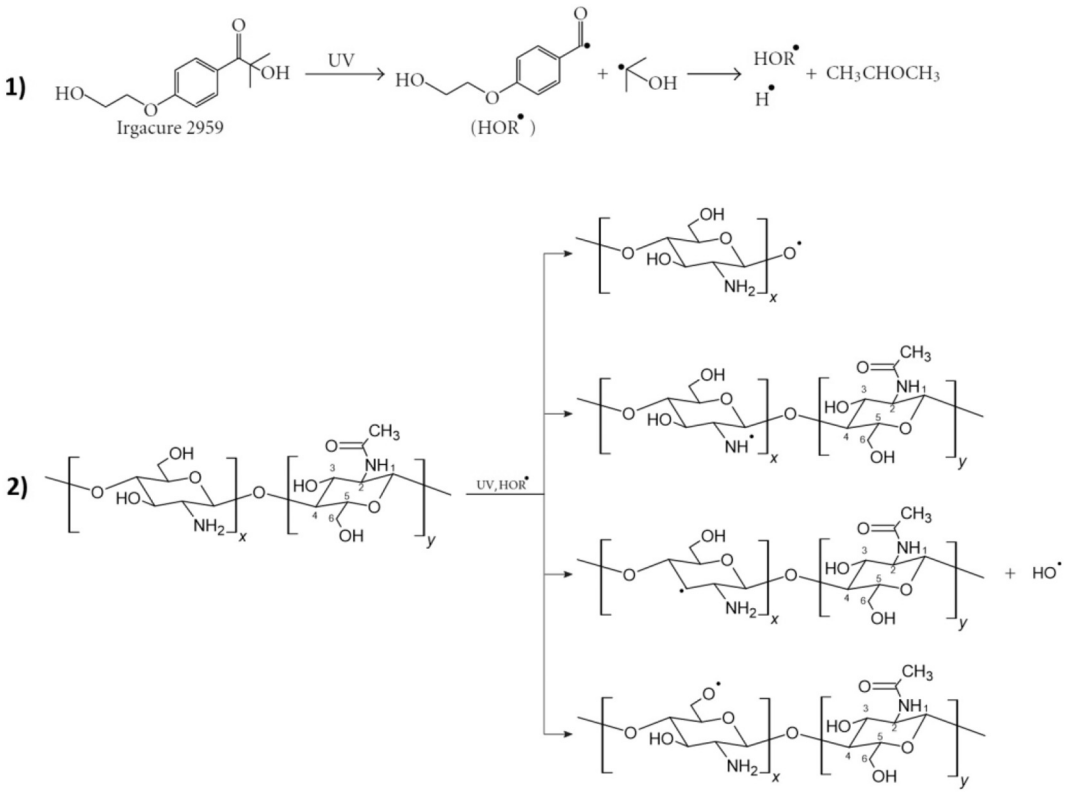

Fig. 5. Formation of chitosan macroradicals initiated by Irgacure 2959.

shown in several studies, high molecular weight polymers or high polymer concentrations, when submitted to TIPS, usually provide smaller inter-connected structures compared to lower molecular weight polymers or lower polymer concentrations (Liang, Wu, Wan, Huang, & Xu, 2013; Matsuyama, Maki, Teramoto, & Asano, 2002). In the TIPS method, temperature and polymer concentration can affect the type of processes occurring in the polymer solution, namely i) nucleation and growth of the polymer rich phase, ii) continuous morphology due to spinodal decomposition and iii) nucleation and growth of a polymer poor phase (van de Witte et al., 1996).

FESEM observations (Fig. 3) clearly evidenced such effects. Indeed, the CS6_Na3 scaffold showed a quite compact structure (Fig. 3C). In general, all of the samples obtained with this procedure possessed a poor porosity and pore interconnection with a low mean pore size (Table 1) not suitable for application in tissue engineering. Therefore, we decided to fix CS concentration at 4%, for which a higher mean pore size was obtained, and to decrease NaOH concentration from 3 to 1 M. Interestingly, the resulting CS4_Na1 possessed a porosity slighter greater than the scaffolds obtained at NaOH 3 M (Fig. 2, $p < 0.05$) as well as a higher mean pore size which resulted of 72 μm vs 35 μm of CS4_Na3 (Table 1, $p < 0.05$). Such findings suggest as freeze-gelation at NaOH 1 M stabilized the open structure obtained by TIPS better than NaOH 3 M, probably as a consequence of a lower kinetics of CS deprotonation which may favor physical interactions among polymer chains (Xu et al., 2017). However, the morphology of the CS4_Na1 scaffold was still quite heterogeneous (Fig. 3D).

Presumably, CS precipitation and structuration occurred not only during the freeze-gelation phase but also during solvent evaporation at room T, thus causing the collapse of the initial structure and partial closure of pores. That is why scaffolds obtained with CS 4% and freeze-gelation with NaOH 1 M were further submitted to freeze-drying in place of drying at room T.

Freeze-drying clearly improved scaffold morphology (Fig. 4). Indeed, the CS4_FD scaffold showed an open structure (Fig. 4B) better than CS4_Na1 (Fig. 4A) in terms of pore size and pore size distribution.

The CS4_FD scaffold showed a pore size distribution narrower than CS4_Na1 (data not shown) and a slightly higher mean pore size (Table 1). The scaffold porosity was also improved from 60% to 85% (Fig. 2, $p < 0.01$). Freeze-drying also affected the scaffold water uptake. Indeed, CS4_FD reached an equilibrium SD of 920 compared to 330 of CS4_Na1 obtained with the same experimental conditions but dried at room T (Table 1).

Photo cross-linking of the CS4_FD scaffold affected only slightly the scaffold swelling degree, which decreased up to a 790 value (Table 1), and the scaffold porosity, which was of ca. 80% for CS4_FD_CL vs 85% of CS4_FD (Fig. 2, $p > 0.05$). Additionally, the crosslinked CS4_FD_CL scaffold had a more homogeneous porous structure (Fig. 4C) with a quite good pore interconnection as observable in the FESEM image taken at higher magnification (Fig. 4D). The CS4_FD_CL scaffold also possessed the highest mean pore size (135 μm, Table 1), suggesting how photo cross-linking efficiently stabilized the scaffold structure avoiding its partial collapse during freeze-drying.

The mechanism of CS crosslinking was in depth investigated by Sionkowska, Wisniewski, Skopinska, Vicini, and Marsano (2005). Specifically, chitosan exposure to UV light causes the formation of macroradicals (Fig. 5), which may interact with each other giving rise to a crosslinked or branched structure. Briefly, UV light can mainly cause hydrogen abstraction, hydroxyl group abstraction, amino group abstraction, and glycidyl bond scission taking place in the C-O-C groups between the tetrahydropyran rings. The presence of a photo-initiator, like Irgacure 2959, can boost the macroradicals formation and enhance the effects of the UV exposure on chitosan structure and properties.

Chitosan scaffold photo cross-linking was qualitatively evaluated by FTIR spectroscopy (Fig. 6A). The ATR-IR spectrum of chitosan presents a characteristic broad absorption band in the range 3000 and 3600 cm^{-1} attributed to the –OH and -NH stretching, the C—H stretching in the range 2980–2780 cm^{-1}, a peak at 1650 cm^{-1} related to the acetylate

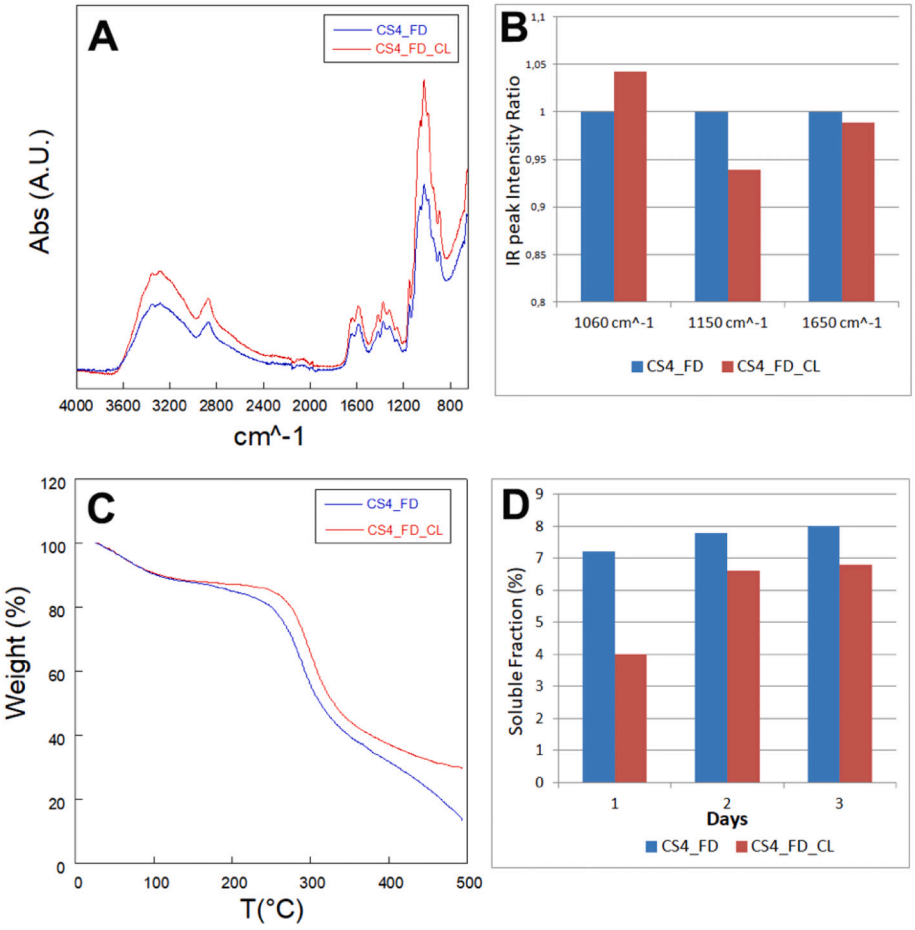

Fig. 6. (A) ATR-IR spectrum of chitosan scaffold before (CS4_FD) and after (CS4_FD_CL) UV irradiation. (B) IR intensity ratio of peaks at 1060 cm^{-1}, 1150 cm^{-1} and 1650 cm^{-1}, after normalization with the peak at 895 cm^{-1}. The IR peaks intensity of the CS scaffold before irradiation was set as 1. (C) Thermogravimetric curve of CS scaffolds before (CS4_FD) and after (CS4_FD_CL) UV irradiation. (D) Soluble fraction of scaffolds in PBS buffer at 37 °C.

groups (amide I), a peak at 1560 cm^{-1} attributed to the N—H bending of primary amines and a peak at 1375 cm^{-1} related to the C—N stretching. Finally, the absorption peaks in the spectral range 1150–1000 cm^{-1} can be attributed to C-O-C and C-O-H stretching and the peak at 895 cm^{-1} to the C-O-C pyranose ring stretching.

After UV irradiation, the IR spectrum of the CS scaffold did not show any new peaks. However, the effect of UV exposure on CS was monitored by comparing the variations in intensity of some FT-IR peak after normalization with the peak at 895 cm^{-1}, which is not influenced by UV irradiation (Sionkowska et al., 2005). Specifically, in the cross-linked scaffold CS4_FD_CL a variation in the intensities of peaks at 1150 cm^{-1} and 1060 cm^{-1} was observed compared to CS4_FD (Fig. 6B), thus confirming how the UV treatment affected the C-O-C and C-O-H bonds as schematized in Fig. 5. Similar findings were reported by Kianfar, Vitale, Dalle Vacche, and Bongiovanni (2019), who investigated the photo-crosslinking of chitosan/polyethyleneoxide electrospun nanofibers.

Thermogravimetric analysis carried out on CS4_FD and CS4_FD_CL scaffolds evidenced an increase in thermal stability of the scaffold after irradiation (Fig. 6C). Specifically, the degradation temperature of the cross-linked scaffold CS4_FD_CL increased by ca. 10 °C, from 287 °C of the uncross-linked scaffold CS4_FD to 298 °C. This higher stability supports the formation of a partially cross-linked chitosan structure following UV irradiation. In line with these data, the soluble fraction of the crosslinked scaffold was slightly lower than that of the CS4_FD (Fig. 6D), especially after 1 day of immersion in water.

In Fig. 7A and B, the mechanical behavior of CS4_FD and CS4_FD_CL scaffolds submitted to compression tests in dried and hydrated state is reported while the compression modulus (CM) of the dried samples, determined by the slope of the initial linear tract of the curve, is reported in Table 1. As expected, in dried state, the cross-linked CS4_FD_CL scaffold showed a compression modulus significantly higher than the CS4_FD scaffold. Specifically, photo cross-linking increased CM by ca. three times reaching a value of ca. 2.2 MPa (Table 1), which is in the order of magnitude of the trabecular bone of some human bones, like the human mandible for which a compression modulus ranging from 0.22 to 10.44 MPa was found (Misch, Qu, & Bidez, 1999). After photo cross-linking, the scaffold compressive strength, taken at a 0.3 compression ratio, also increased from 0.25 to 0.65 MPa, evidencing a better resistance to failure of the crosslinked CS4_FD_CL scaffold. Additionally, both dried scaffolds showed a yield point at a 0.4 compression ratio (Fig. 7A), which is a significantly high value for the application (Oftadeh, Perez-Viloria, Villa-Camacho, Vaziri, & Nazarian, 2015). Interestingly, the yield point was not evident on the curves of the hydrated samples (Fig. 7B), presumably because in the swollen state, water molecules filling the pores may provide elasticity increasing the material elastic, reversible zone, as shown by Gorczyca et al. (2014). However, a decrease in stiffness was observed following hydration, the compression modulus decreasing up to 0.7 and 0.5 MPa for CS4_FD and CS4_FD_CL, respectively. This is a known phenomenon probably caused by the weakening of hydrogen bonds within the chitosan molecular structure induced by water interaction with the biopolymer itself (Varley et al., 2016). Indeed, in hydrophilic polymers, water molecules can establish hydrogen bonds with the polymer polar groups and interpose within the polymer chains, thus weakening the inter- and intra-molecular

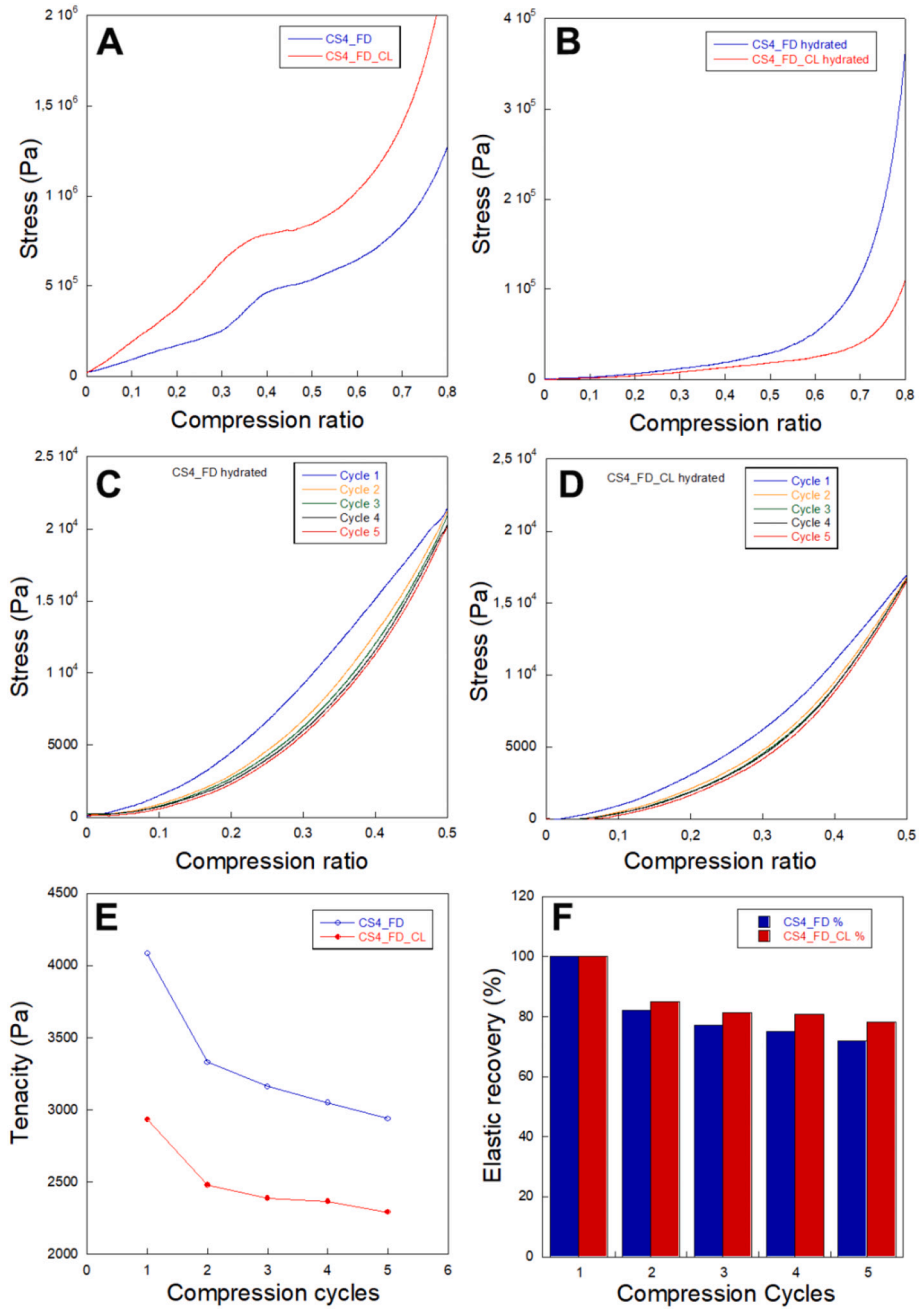

Fig. 7. Stress strain curves of scaffolds obtained with 4% CS concentration, freeze-dried (CS4_FD) or photo cross-linked and freeze-dried (CS4_FD_CL), measured in a dried (A) or hydrated state (B). Compression cycles for CS4_FD (C) and CS4_FD_CL (D) hydrated scaffolds. Tenacity (E) and elastic recovery (F) of CS4_FD and CS4_FD_CL hydrated scaffolds submitted to five compression cycles.

interactions among polymer chains. Polymer chains separated in this way are far more easily moved relative to one another than when they are bonded closely. In short, water can act as plasticizing molecules.

In general, the mechanical performance of our scaffolds can be considered greatly satisfying if compared with those showed by pure chitosan scaffolds, obtained similarly without any additive, but prepared with different fabrication processes (Albanna et al., 2012; Hsieh et al., 2007; Xu et al., 2017). Particularly, Albanna et al. (2012) prepared chitosan scaffolds reinforced with crosslinked chitosan fibers having an elastic modulus tensile strength in the KPa order of magnitude, 70 KPa and 58 KPa respectively. Hsieh et al. (2007) developed reinforced chitosan scaffolds by freeze gelation in different conditions, reaching tensile strengths ranging from 30 to 180 KPa. Finally, Xu et al. (2017) fabricated high mechanical strength chitosan scaffolds by chitosan neutralization in NaOH/NaCl solution under compression at different ratios, obtaining the best compression modulus (500 KPa) and strength (3 KPa) for scaffolds obtained at a compression ratio of 8.

The hydrated samples were then submitted to a series of compression cycles to investigate the fatigue life (Fig. 7C and D). From these curves, the tenacity and the elastic recovery were determined. As it can be observed, in both scaffolds, the tenacity decreased by ca. 30% in the second compression cycle (Fig. 7E), while remained substantially constant for the rest of the cycles, especially in the case of CS4_FD_CL. This latter showed therefore the best elastic response which resulted of 80% up to five compression cycles (Fig. 7F).

Besides the absolute compression modulus and strength, a good elastic response is very important for substitution of trabecular bone tissues submitted to cyclic stresses. Indeed, it is known that, although

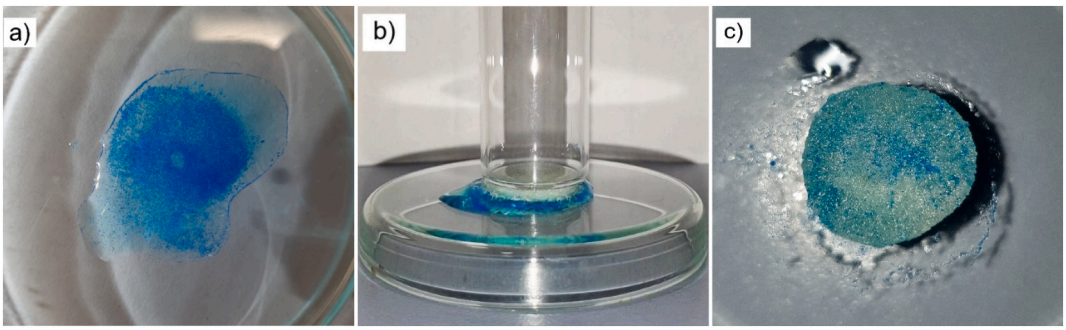

Fig. 8. Images showing the penetration of alginate microsphere (100 μm) into the structure of the CS4_FD_CL porous structure by "sponge effect".

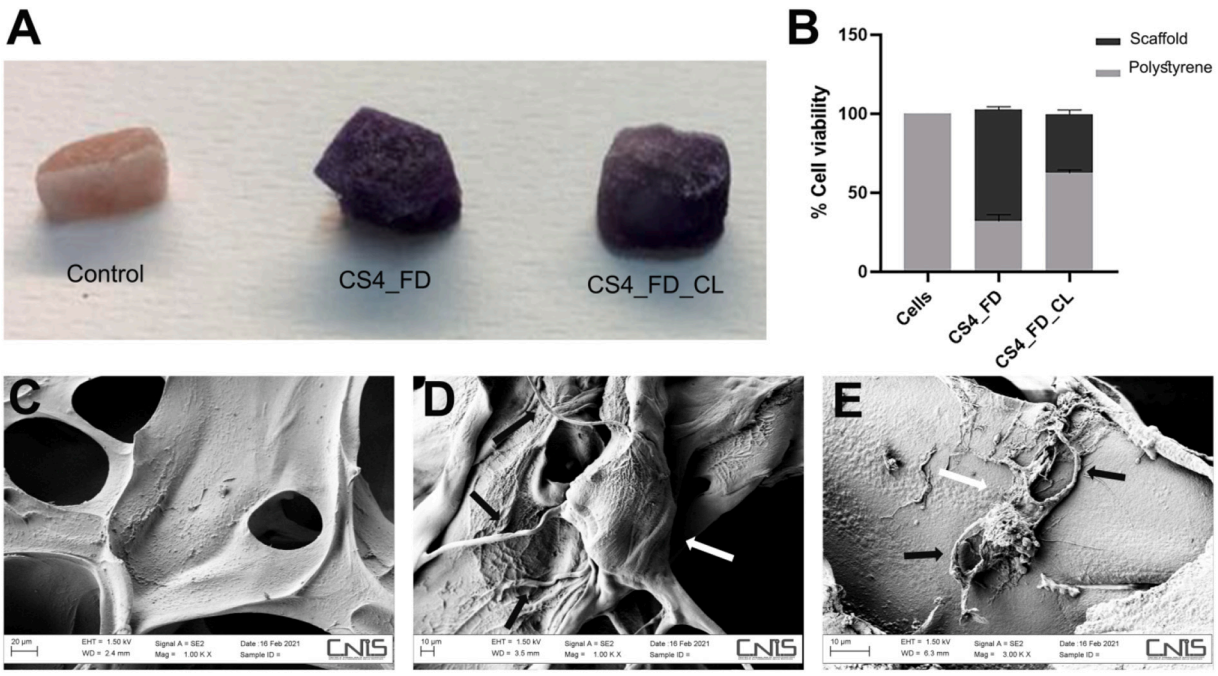

Fig. 9. (A) Images of MTS-stained CS4_FD scaffold not seeded with osteoblasts (control) and CS4_FD scaffold and CS4_FD_CL after seeding and incubation with osteoblasts. Cells were seeded into the scaffolds by sponge effect, applying a mechanical pressure. (B) Cell viability of osteoblasts seeded into CS4_FD and CS4_FD_CL scaffolds, assessed by MTS assay. Cells seeded in 96 well cell culture plate were considered the negative control 100% viability (light gray histogram). Cells adsorbed into the scaffolds are represented by dark gray, cells remained into cell culture plate, polystyrene, are represented by light gray. (C, D, E) FESEM micrographs of CS4_FD_CL without cells (C) at 1000× magnification, of osteoblasts seeded into CS4_FD (D) and CS4_FD_CL (E) scaffolds, at 1000× and 3000× magnification, respectively. White and black arrows indicate cell body and actin filaments, respectively. All the experiments were performed in triplicate.

the trabecular bone can sustain compressive strains up to 50%, largely over its yield point occurring approximately at 0.7% strains in compression, when compressed beyond its yield point, unloaded, and reloaded, permanent residual strains and loss of strength occur (Morgan, Unnikrisnan, & Hussein, 2018). Such cumulative permanent deformations could lead in the long-term to clinical fracture.

The good elastic response of the hydrated CS4_FD and CS4_FD_CL scaffolds could be also used to permit permeability of cells within the scaffold by the application of an external pressure ("sponge effect" mechanism). Indeed, scaffold cell seeding is a quite delicate phase since cells tend to colonize the scaffold surface instead of penetrating inside the scaffold structure. To date, the most common seeding technique is the static seeding, in which a concentrated cell suspension is passively introduced onto a scaffold. However, such method often results in a low seeding efficiency and minimal cell penetration into the scaffold walls (Villalona et al., 2010). Recently, Bai and colleagues (Bai et al., 2015) developed ceramic scaffolds with gradient channel structures in order to seed cells by capillary effect. To preliminarily verify the feasibility of the proposed seeding technique by sponge effect, scaffold ability to adsorb a suspension of alginate microparticles with a mean size (100 μm), comparable to osteoblast cell size, by one cycle of mechanical loading and unloading. To visualize microparticles penetration within the scaffold, a blue dye (FCF Brilliant Blue) was entrapped in to the alginate microparticles. As can be observed in Fig. 8, the CS4_FD_CL scaffold was able to absorb efficiently the 500 μL microparticles suspension, permitting penetration of microparticles within all of the scaffold structure up to the superior scaffold surface (Fig. 8C).

The validity of seeding method was then confirmed by using concentrated osteoblast suspensions (Fig. 9).

Cells efficiently penetrated into both CS4_FD and CS4_FD_CL scaffolds, confirming the suitability of the scaffold topography to house osteoblasts. Additionally, scaffolds' staining with the MTS dye showed a good viability of the penetrated cells as evidenced by the intense coloration taken by the scaffolds seeded with osteoblasts compared to the scaffold not seeded with cells (Fig. 9A). This result was confirmed by measuring the spectrophotometric absorbance of both CS4_FD and CS4_FD_CL scaffolds seeded with cells (Fig. 9B), taking as 100% cell viability the optical density measured in cells directly seeded into cell

culture plate without scaffold (light gray histogram). We observed that a certain amount of cells remained in the bottom of the wells containing the scaffolds. In particular, the number of cells in the well bottom was higher in the CS4_FD_CL compared to CS4_FD wells ($p < 0.05$), according to the larger diameter of the pores in CS4_FD_CL (140 μm) with respect to CS4_FD (100 μm). The optical absorbance of the cells remained into the well was also measured, confirming that the scaffolds are not detrimental for cell viability (Fig. 9B).

Finally, in order to observe the cells seeded into the scaffolds, we performed a scanning electron microscope analysis, finding that the cells were perfectly visible both in CS4_FD and CS4_FD_CL scaffolds (Fig. 9D, E). In the same figure, the structure of CS4_FD_CL not seeded with cells is also shown (Fig. 9C). Adhered osteoblast cells have a typical elongated and stretched morphology (Lopreiato et al., 2020). Cells have also started producing many and long actin filaments, which are required for interaction with scaffold. The presence of actin filaments and membrane protrusions suggest a good metabolic activity of cells following interaction with the scaffold.

4. Conclusions

In summary, a scaffold fabrication method was efficiently setup allowing the obtainment of chitosan scaffolds with mechanical properties and topography suitable for tissue regeneration of trabecular bone. The open structure was obtained by TIPS and the effect of chitosan concentration, freeze-gelation and drying conditions on the scaffold morphology and physical performance were investigated. Results confirmed the crucial role of freeze drying to obtain a highly porous structure and, as hypothesized, evidenced how the combination of freeze-gelation and photo crosslinking may permit to improve mechanical resistance of the scaffolds, which exhibited a compression modulus with the same order of magnitude of some types of human trabecular bones. Scaffolds also showed a good fatigue life which may permit their use for substitution of bone tissues submitted to cyclic stress. We also demonstrated how the elastic properties of the scaffolds may be used to permit an efficient cell seeding and penetration into the scaffold structure. The herein reported method does not require external cross-linking agents, sophisticated instrumentation, and could be conveniently extended to other soft materials.

Funding

This work was supported by the Sapienza University of Rome through a grant to I.F.

CRediT authorship contribution statement

Ilaria Silvestro: Formal analysis, Investigation. **Riccardo Sergi:** Formal analysis, Investigation. **Anna Scotto D'Abusco:** Formal analysis, Writing – review & editing. **Alessia Mariano:** Formal analysis, Investigation. **Andrea Martinelli:** Investigation, Data curation. **Antonella Piozzi:** Data curation, Writing – review & editing. **Iolanda Francolini:** Conceptualization, Data curation, Writing – original draft, Funding acquisition.

References

Aguilar, A., Zein, N., Harmouch, E., Hafdi, B., Bornert, F., Offner, D., … Hua, G. (2019). Application of chitosan in bone and dental engineering. *Molecules, 24*(16), 3009. https://doi.org/10.3390/molecules24163009

Albanna, M. Z., Bou-Akl, T. H., Blowytsky, O., & Matthew, H. W. (2012). Chitosan fibers with improved biological and mechanical properties for tissue engineering applications. *Journal of the Mechanical Behavior of Biomedical Materials, 20*(4), 217–226. https://doi.org/10.1016/j.jmbbm.2012.09.012

Amato, A., Migneco, L. M., Martinelli, A., Pietrelli, L., Piozzi, A., & Francolini, I. (2018). Antimicrobial activity of catechol functionalized-chitosan versus *Staphylococcus epidermidis*. *Carbohydrate Polymers, 179*, 273–281. https://doi.org/10.1016/j.carbpol.2017.09.073

Arumugam, S., Kandasamy, J., Md Shah, A. U., Sultan, M. T. H., Safri, S. N. A., Majid, M. S. A., … Mustapha, F. (2020). Investigations on the mechanical properties of glass fiber/sisal fiber/chitosan reinforced hybrid polymer sandwich composite scaffolds for bone fracture fixation applications. *Polymers, 12*(7), Article E1501. https://doi.org/10.3390/polym12071501

Bai, H., Wang, D., Delattre, B., Gao, W., De Coninck, J., Li, S., & Tomsia, A. P. (2015). Biomimetic gradient scaffold from ice-templating for self-seeding of cells with capillary effect. *Acta Biomaterialia, 20*, 113–119. https://doi.org/10.1016/j.actbio.2015.04.007

Bhattarai, N., Edmondson, D., Veiseh, O., Matsen, F. A., & Zhang, M. (2005). Electrospun chitosan-based nanofibers and their cellular compatibility. *Biomaterials, 26*(31), 6176–6184. https://doi.org/10.1016/j.biomaterials.2005.03.027

Chollakup, R., Uttayarat, P., Chworos, A., & Smitthipong, W. (2020). Noncovalent sericin-chitosan scaffold: Physical properties and low cytotoxicity effect. *International Journal of Molecular Science, 21*(3), 775. https://doi.org/10.3390/ijms21030775

Cuzzucoli Crucitti, V., Migneco, L. M., Piozzi, A., Taresco, V., Garnett, M., Argent, R. H., & Francolini, I. (2018). Intermolecular interaction and solid state characterization of abietic acid/chitosan solid dispersions possessing antimicrobial and antioxidant properties. *European Journal of Pharmaceutics and Biopharmaceutics, 125*, 114–123. https://doi.org/10.1016/j.ejpb.2018.01.012

Dado, D., & Levenberg, S. (2009). Cell-scaffold mechanical interplay within engineered tissue. *Seminars in Cell and Developmental Biology, 20*(6), 656–664. https://doi.org/10.1016/j.semcdb.2009.02.001

Esmaeili Pourfarhangi, K., Mashayekhan, S., Asl, S. G., & Hajebrahimi, Z. (2018). Construction of scaffolds composed of acellular cardiac extracellular matrix for myocardial tissue engineering. *Biologicals, 53*, 10–18. https://doi.org/10.1016/j.biologicals.2018.03.005

Francolini, I., Donelli, G., Crisante, F., Taresco, V., & Piozzi, A. (2015). Antimicrobial polymers for anti-biofilm medical devices: State-of-art and perspectives. *Advances in Experimental Medicine and Biology, 831*, 93–117. https://doi.org/10.1007/978-3-319-09782-4_7

Francolini, I., Perugini, E., Silvestro, I., Lopreiato, M., Scotto d'Abusco, A., Valentini, F., … Piozzi, A. (2019). Graphene oxide oxygen content affects physical and biological properties of scaffolds based on chitosan/graphene oxide conjugates. *Materials, 12*(7), 1142. https://doi.org/10.3390/ma12071142

Gorczyca, G., Tylingo, R., Szweda, P., Augustin, E., Sadowska, M., & Milewski, S. (2014). Preparation and characterization of genipin cross-linked porous chitosan–collagen–gelatin scaffolds using chitosan–CO2 solution. *Carbohydrate Polymers, 102*, 901–911. https://doi.org/10.1016/j.carbpol.2013.10.060

Hsieh, C. Y., Tsai, S. P., Ho, M. H., Wang, D. M., Liu, C. E., Hsieh, C. H., … Hsieh, H. J. (2007). Analysis of freeze-gelation and cross-linking processes for preparing porous chitosan scaffolds. *Carbohydrate Polymers, 67*(1), 124–132. https://doi.org/10.1016/j.carbpol.2006.05.002

Jabbari, F., Hesaraki, S., & Houshmand, B. (2019). The physical, mechanical, and biological properties of silk fibroin/chitosan/reduced graphene oxide composite membranes for guided bone regeneration. *Journal of Biomaterial Science Polymer Ed., 30*(18), 1779–1802. https://doi.org/10.1080/09205063.2019.1666235

Jayakumar, R., Prabaharan, M., Nair, S. V., & Tamura, H. (2010). Novel chitin and chitosan nanofibers in biomedical applications. *Biotechnology Advances, 28*(1), 142–150. https://doi.org/10.1016/j.biotechadv.2009.11.001

Kianfar, P., Vitale, A., Dalle Vacche, S., & Bongiovanni, R. (2019). Photo-crosslinking of chitosan/poly(ethylene oxide) electrospun nanofibers. *Carbohydrate Polymers, 217*, 144–151. https://doi.org/10.1016/j.carbpol.2019.04.062

Kim, I. Y., Seo, S. J., Moon, H. S., Yoo, M. K., Park, I. Y., Kim, B. C., & Cho, C. S. (2008). Chitosan and its derivatives for tissue engineering applications. *Biotechnology Advances, 26*(1), 1–21. https://doi.org/10.1016/j.biotechadv.2007.07.009

Liang, H. Q., Wu, Q. Y., Wan, L. S., Huang, X. J., & Xu, Z. K. (2013). Polar polymer membranes via thermally induced phase separation using a universal crystallizable diluents. *Journal of Membrane Science, 446*, 482–491. https://doi.org/10.1016/j.memsci.2013.07.008

Lopreiato, M., Mariano, A., Cocchiola, R., Longo, G., Dalla Vedova, P., Scandurra, R., & Scotto d'Abusco, A. (2020). Nanostructured TiC layer is highly suitable surface for adhesion, proliferation and spreading of cells. *Condensed Matter, 5*, 29.

Ma, L., Gao, C., Mao, Z., Shen, J., Hu, X., & Han, C. (2003). Thermal dehydration treatment and glutaraldehyde cross-linking to increase the biostability of collagen-chitosan porous scaffolds used as dermal equivalent. *Journal of Biomaterial Science Polymer Ed., 14*(8), 861–874. https://doi.org/10.1163/156856203768366576

Matsuyama, H., Maki, T., Teramoto, M., & Asano, K. (2002). Effect of polypropylene molecular weight on porous membrane formation by thermally induced phase separation. *Journal of Membrane Science, 204*(1–2), 323–328. https://doi.org/10.1016/S0376-7388(02)00056-X

Misch, C. E., Qu, Z., & Bidez, M. W. (1999). Mechanical properties of trabecular bone in the human mandible: Implications for dental implant treatment planning and surgical placement. *Journal of Oral and Maxillofacial Surgery, 57*(6), 700–708. https://doi.org/10.1016/S0278-2391(99)90437-8

Morgan, E. F., Unnikrisnan, G. U., & Hussein, A. I. (2018). Bone mechanical properties in healthy and diseased states. *Annual Review of Biomedical Engineering, 20*, 119–143. https://doi.org/10.1146/annurev-bioeng-062117-121139

Nam, Y. S., & Park, T. G. (1999). Porous biodegradable polymeric scaffolds prepared by thermally induced phase separation. *Journal of Biomedical Materials Research, 47*(1), 8–17. https://doi.org/10.1002/(SICI)1097-4636(199910)47:1<8::AID-JBM2>3.0.CO;2-L

Oftadeh, R., Perez-Viloria, M., Villa-Camacho, J. C., Vaziri, A., & Nazarian, A. (2015). Biomechanics and mechanobiology of trabecular bone: A review. *Journal of*

Biomechanical Engineering, 137(1), 0108021–01080215. https://doi.org/10.1115/1.4029176

Pakornpadungsit, P., Prasopdee, T., Swainson, N. M., Chworos, A., & Smitthipong, W. (2020). DNA:Chitosan complex, known as a drug delivery system, can create a porous scaffold. *Polymer Testing, 83*, 106333. https://doi.org/10.1016/j.polymertesting.2020.106333

Pineda-Castillo, S., Bernal-Ballén, A., Bernal-López, C., Segura-Puello, H., Nieto-Mosquera, D., Villamil-Ballesteros, A., … Munster, L. (2018). Synthesis and characterization of poly(vinyl alcohol)-chitosan-hydroxyapatite scaffolds: A promising alternative for bone tissue regeneration. *Molecules, 23*(10), 2414. https://doi.org/10.3390/molecules23102414

Seol, Y. J., Lee, J. Y., Park, Y. J., Lee, Y. M., Ku, Y., Rhyu, I. C., … Chung, C. P. (2004). Chitosan sponges as tissue engineering scaffolds for bone formation. *Biotechnology Letters, 26*(13), 1037–1041. https://doi.org/10.1023/B:BILE.0000032962.79531.fd

Silvestro, I., Lopreiato, M., Scotto d'Abusco, A., Di Lisio, V., Martinelli, A., Piozzi, A., & Francolini, I. (2020). Hyaluronic acid reduces bacterial fouling and promotes fibroblasts' adhesion onto chitosan 2d-wound dressings. *International Journal of Molecular Science, 21*(6), 2070. https://doi.org/10.3390/ijms21062070

Sionkowska, A., Wisniewski, M., Skopinska, J., Vicini, S., & Marsano, E. (2005). The influence of UV irradiation on the mechanical properties of chitosan/poly(vinyl pyrrolidone) blends. *Polymer Degradation and Stability, 88*(2), 261–267. https://doi.org/10.1016/j.polymdegradstab.2004.08.018.

van de Witte, P., Dijkstra, P. J., van den Berg, J. W. A., & Feijen, J. (1996). Phase separation processes in polymer solutions in relation to membrane formation. *Journal of Membrane Science, 117*, 1–31. https://doi.org/10.1016/0376-7388(96)00088-9

Varley, M. C., Neelakantan, S., Clyne, T. W., Dean, J., Brooks, R. A., & Markaki, A. E. (2016). Cell structure, stiffness and permeability of freeze-dried collagen scaffolds in dry and hydrated states. *Acta Biomaterialia, 33*, 166–175. https://doi.org/10.1016/j.actbio.2016.01.041

Venkatesan, J., & Kim, S. K. (2010). Chitosan composites for bone tissue engineering-an overview. *Marine Drugs, 8*(8), 2252–2266. https://doi.org/10.3390/md8082252

Villalona, G. A., Udelsman, B., Duncan, D. R., McGillicuddy, E., Sawh-Martinez, R. F., Hibino, N., … Breuer, C. K. (2010). Cell-seeding techniques in vascular tissue engineering. *Tissue Engineering Part B: Reviews, 16*(3), 341–350. https://doi.org/10.1089/ten.teb.2009.0527

Wang, W., Meng, Q., Li, Q., Liu, J., Zhou, M., Jin, Z., & Zhao, K. (2020). Chitosan derivatives and their application in biomedicine. *International Journal of Molecular Science, 21*(2), 487. https://doi.org/10.3390/ijms21020487

Wu, S. W., Liu, X., Miller, A. L., 2nd, Cheng, Y. S., Yeh, M. L., & Lu, L. (2018). Strengthening injectable thermo-sensitive NIPAAm-g-chitosan hydrogels using chemical cross-linking of disulfide bonds as scaffolds for tissue engineering. *Carbohydrate Polymers, 192*, 308–316. https://doi.org/10.1016/j.carbpol.2018.03.047

Xu, Y., Han, J., Chai, Y., Yuan, S., Lin, H., & Zhang, X. (2018). Development of porous chitosan/tripolyphosphate scaffolds with tunable uncross-linking primary amine content for bone tissue engineering. *Materials Science and Engineering C, 85*, 182–190. https://doi.org/10.1016/j.msec.2017.12.032

Xu, Y., Xia, D., Han, J., Yuan, S., Lin, H., & Zhao, C. (2017). Design and fabrication of porous chitosan scaffolds with tunable structures and mechanical properties. *Carbohydrate Polymers, 177*, 210–216. https://doi.org/10.1016/j.carbpol.2017.08.069

Zeng, S., Liu, L., Shi, Y., Qiu, J., Fang, W., Rong, M., … Gao, W. (2015). Characterization of silk fibroin/chitosan 3D porous scaffold and in vitro cytology. *PLoS One, 10*(6), Article e0128658. https://doi.org/10.1371/journal.pone.0128658